frontiers in Materials

ORIGINAL RESEARCH
published: 08 May 2020
doi: 10.3389/fmats.2020.00100

Magnetic Carbon Nanotubes/Graphene Oxide Nanocomposites: One-Step Controllable Production, and Their Excellent Microwave Absorption Capabilities

Mei Wu[1], Xiaosi Qi[1,2,3]†, Ren Xie[1], Shuijie Qin[1], Chaoyong Deng[2] and Wei Zhong[3]†*

[1] College of Physics, Guizhou Province Key Laboratory for Photoelectrics Technology and Application, Guizhou University, Guiyang, China, [2] Key Laboratory of Electronic Composites of Guizhou Province, Guizhou University, Guiyang, China, [3] National Laboratory of Solid State Microstructures and Jiangsu Provincial Laboratory for NanoTechnology, Nanjing University, Nanjing, China

OPEN ACCESS

Edited by:
Biao Zhao,
Zhengzhou University of Aeronautics, China

Reviewed by:
Guanglei Wu,
Qingdao University, China
Yaofeng Zhu,
Zhejiang Sci-Tech University, China
Yongxing Zhang,
Huaibei Normal University, China

***Correspondence:**
Xiaosi Qi
xsqi@gzu.edu.cn

†ORCID:
Xiaosi Qi
orcid.org/0000-0003-0987-1622
Wei Zhong
orcid.org/0000-0003-2507-3479

Specialty section:
This article was submitted to Polymeric and Composite Materials, a section of the journal Frontiers in Materials

Received: 23 February 2020
Accepted: 31 March 2020
Published: 08 May 2020

Citation:
Wu M, Qi X, Xie R, Qin S, Deng C and Zhong W (2020) Magnetic Carbon Nanotubes/Graphene Oxide Nanocomposites: One-Step Controllable Production, and Their Excellent Microwave Absorption Capabilities. Front. Mater. 7:100. doi: 10.3389/fmats.2020.00100

In this research, three-dimensional (3D) hierarchical networks of magnetic carbon nanotubes/graphene oxide (CNTs/GO) nanocomposites (NCs) were synthesized by a one-step hydrothermal method with the idea of constructing more interface contacts, a double loss mechanism and synergy effect. The obtained results showed that the content of NCs gradually transitioned from $CoCO_3$ to $Co_xFe_{3-x}O_4$. Further, $CoCO_3$-$Co_xFe_{3-x}O_4$/CNTs/GO quaternary NCs and $Co_xFe_{3-x}O_4$/CNTs/GO ternary NCs could be selectively synthesized when the Co:Fe molar ratio decreased from 1:1 to 1:3. The as-prepared samples displayed excellent microwave absorption properties (MAPs) in terms of the minimum reflection loss (RL_{min}) and the corresponding absorption bandwidth (FB_{cor}) with reflection loss values lower than −10 dB. The RL_{min} and large FB_{cor} values for the as-prepared samples were −54.69 dB and 2.36 GHz, −63.99 dB and 2.48 GHz, −63.36 dB and 2.68 GHz, respectively. The designed 3D hierarchical networked structure of magnetic GO/CNTs NCs displayed outstanding comprehensive MAPs, which could deliver a practical and effective strategy to develop high-performance microwave absorbers (MAs), considering their low cost, lightweight, and high stability.

Keywords: magnetic GO/CNTs, 3D hierarchical networks structure, interfacial polarizations, dielectric and magnetic loss mechanisms, microwave absorption properties

INTRODUCTION

In the past decades, microwave absorbers (MAs) have drawn significant attention owing to the expanded electromagnetic (EM) radiation and interference problems (Novoselov et al., 2004; Zhang et al., 2014; Cao et al., 2019). It is well acknowledged that MAs with characteristics such as strong absorption ability, large absorption bandwidth, lightweight, low cost, and remarkable chemical stability are highly desirable because of their promising military and civil application prospects

(Zhang et al., 2015; Fang et al., 2016). According to the EM energy conversion principle, the incident EM wave can be attenuated by dielectric and magnetic losses (Wei et al., 2017). Therefore, nanocomposites (NCs) consisting of dielectric loss materials and magnetic nanoparticles (NPs) are considered an effective way to achieve high-performance MAs (Liu et al., 2015, 2018; Quan et al., 2017). For example, CoNi@Air@TiO_2 (Liu et al., 2016), $Co_{0.6}Fe_{2.4}O_4$@MoS_2 (Long et al., 2019), Ni@SnO_2 (Zhao et al., 2016), Co_7Fe_3@SiO_2 (Chen et al., 2017) have been demonstrated to display outstanding microwave absorption properties (MAPs). Generally, owing to their excellent synergistic effect, the development of high-performance MAs mainly focused on core@shell structure magnetic NCs, in which dielectric substances are utilized as a shell and magnetic NPs as a core. Among them, different dielectric substances such as ZnO, TiO_2, and $BaTiO_3$ were often used as a shell (Liu et al., 2008; Jiang et al., 2014; Xu et al., 2018). However, the biggest drawback of these NCs is the high density, which hugely restricts their practical application.

In recent years, owing to the lightweight, unique tube structure and excellent dielectric loss, carbon nanotubes (CNTs) were used as substrate to construct the CNTs-based for designing the ideal MAs (Chen et al., 2015; Wang et al., 2018). Examples include Fe/CNTs (Che et al., 2004), $ZnFe_2O_4$/CNTs (Khabouri et al., 2015), and Fe/Co/Ni/CNTs (Wen et al., 2011), which were demonstrated to display very outstanding MAPs. Generally, the previously designed core@shell structure CNTs-based NCs were mainly composed of CNTs as a shell and different categories of magnetic NPs as a core (Lv et al., 2008; Weissker et al., 2010). However, the magnetic properties and magnetic loss abilities for these kinds of CNTs-based NCs are hugely limited and cannot be well modulated due to the magnetic NPs acting as the core, and the low encapsulation of magnetic NPs (Pawar et al., 2019; Long et al., 2020). Therefore, constructing the reverse core@shell structure magnetic CNTs-based NCs, in which magnetic NPs serve as the shell and CNTs as the core, is an effective way to overcome these problems (Wang et al., 2012; Li et al., 2017).

Furthermore, the recent results indicated that the outstanding properties of graphene (G) and the designed G-based could provide many more interfaces, which were conducive to improve MAPs (Qu et al., 2016; Wang et al., 2019). Considering these aspects, in this article, we designed and synthesized magnetic CNTs/graphene oxide (GO) NCs by a one-step hydrothermal method. By changing the Co:Fe molar ratio, different compositions of magnetic NPs/CNTs/GO NCs could be selectively produced. The obtained results showed that the as-prepared magnetic CNTs/GO NCs displayed very excellent MAPs.

EXPERIMENTAL

Synthesis of Magnetic CNTs/GO NCs

Similarly to the previously reported experimental method shown in **Figure 1** (Wu et al., 2020), 80 mg of GO was prepared by a modified Hummers method (Hummers and Offeman, 1958). The prepared GO was added in 40 mL deionized water and ultrasonicated for 30 min at room temperature (RT). Next, 40 mg of hydroxylated CNTs were ultrasonically dispersed into the GO solution for another 30 min to obtain the GO/CNTs substrate solution. Then, the solution of Co^{2+} and Fe^{3+} was obtained by ultrasonic dissolving $C_4H_6CoO_4 \bullet 4H_2O$ (1 mmol) and $FeCl_3 \bullet 6H_2O$ (1 mmol) into a 30 mL ethylene glycol solution. Subsequently, the resulting Co^{2+} and Fe^{3+} solution was dissolved into GO/CNTs substrate solution by stirred for ca. 60 min. Finally, urea (0.9 g) were thoroughly dispersed into the mixed solution for another 5 min. The final solution was transferred into a 100 mL Teflon-lined stainless steel autoclave and heated at 200°C for 24 h and left to cool to RT. The synthesized magnetic CNTs/GO NCs were washed several times and magnetically centrifuged. The obtained sample was left to dry. The experimental conditions were kept the same, with the exception of 2 and 3 mmol of $FeCl_3 \bullet 6H_2O$, which were used as the Fe source in the synthesis of magnetic NPs/CNTs/GO NCs to control compositions of the sample. The samples were denoted as S1, S2, and S3 for easy description, respectively.

Characterization and Measurement

The phases and microstructures of the as-prepared magnetic CNTs/GO NCs were characterized by an X-ray powder diffractometer (XRD) (model Smart Lab, Rigaku), Raman spectroscopy (Jobin-Yvon Labram HR800), Thermal gravity analysis (TGA) (Netzsch Sta 449F3), transmission electron microscope (TEM) (model Tecnai-G20), and X-ray photoelectron spectroscopy (XPS) (model Escalab 250Xi, Thermo Fisher Scientific). 30 wt% of the obtained samples were mixed with wax and pressed into toroidal shaped samples (R_{out}: 7.0 mm, R_{in}: 3.0 mm), respectively, to investigate the EM properties and MAPs. The as-prepared composites were measured by a vector network analyzer (Agilent E8363B) in the frequency region of 2–18 GHz.

RESULTS AND DISCUSSION

Figure 2 presents the XRD patterns and Raman spectra of the as-prepared magnetic CNTs/GO NCs. **Figure 2A** shows that all the as-prepared samples display similar XRD patterns, pointing to the same category of sample. The characteristic peaks at 30.08°, 35.44°, 43.06°, 53.44°, 56.97° and 62.59° corresponding to (220), (311), (400), (422), (511), and (440) crystal planes are consistent with the standard XRD patterns of spinel $CoFe_2O_4$ (JCPDS: 22-1086). In comparison, one peak at 32.6° can be observed clearly over S1 and S2, assigned to (104) crystal planes of $CoCO_3$ (JCPDS: 78-0209). However, this peak cannot be seen over sample S3. The comparison results reveal that the obtained samples evolve from $CoCO_3$ to $Co_xFe_{3-x}O_4$ when the amount of Fe source increases from 1 mmol to 3 mmol. In confirmation of the results, the experimental conditions were kept the same, with the exception of 5 mmol $FeCl_3 \bullet 6H_2O$, which was used as the Fe source to produce the sample, S4 for easy description. As shown in **Figure 2A**, the XRD pattern indicates that the phase of $CoCO_3$ cannot be observed over the as-prepared S4, which is consistent with our previous reported result

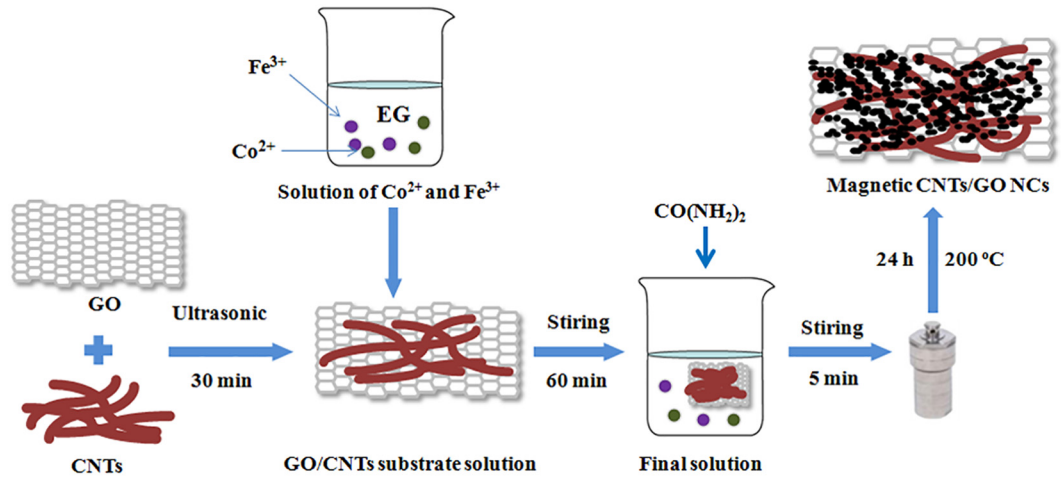

FIGURE 1 | Schematic illustration for the synthesis process of the as-prepared magnetic CNTs/GO NCs.

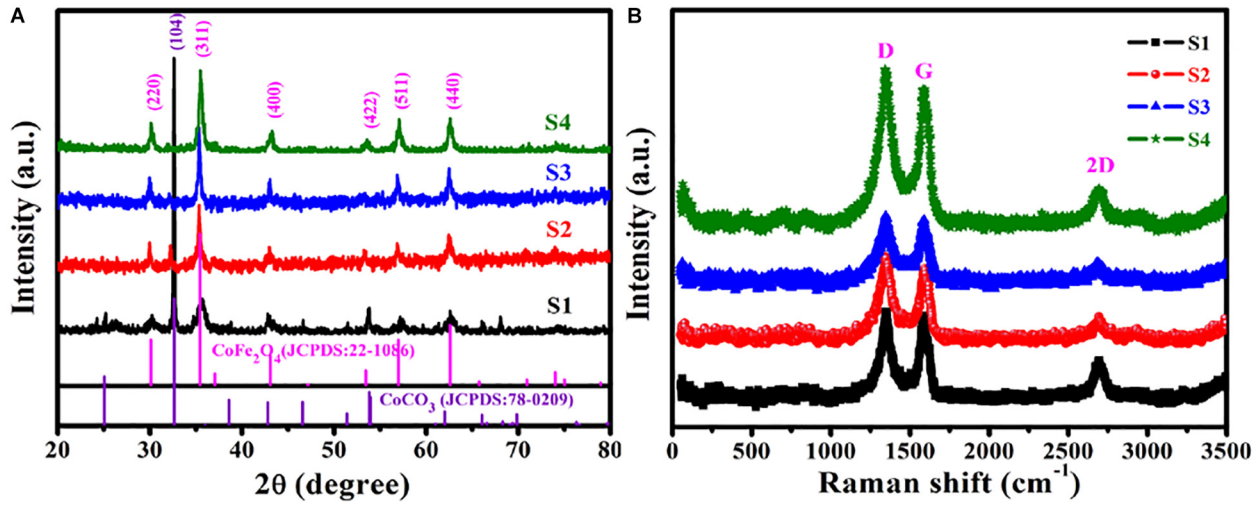

FIGURE 2 | (A) XRD patterns, and **(B)** Raman spectra of the as-prepared samples.

(Wu et al., 2020). Moreover, consistent with the GO/CNT-Fe_3O_4 NCs reported elsewhere (Wang et al., 2014), the characteristic diffraction peaks for GO and CNTs cannot be seen, which should be attributed to the uniform dispersion of $Co_xFe_{3-x}O_4$ NPs on the surface of CNTs/GO. The existence of carbon materials can be confirmed by Raman spectra. As shown in **Figure 2B**, the obtained magnetic CNTs/GO NCs show three evident peaks located at 1347 cm^{-1}, 1586 cm^{-1}, and 2694 cm^{-1}, respectively. These peaks can correspond to the D band, G band and 2D band of carbon material, respectively. It is well-known that the D band originates from the sp^3 defect/disorder in the graphitic structure, the G band is indicative of a high crystallinity graphitic layer, and the 2D band is excited by a double-resonant Raman process (Ritter et al., 2006; Popov and Lambin, 2013). Based on the obtained results, we can confirm the existence of GO and CNTs in the obtained NCs.

Figure 3 shows the typical TGA curves and XPS spectra of as-prepared samples. As shown in **Figure 3A**, it can be seen that the obtained S2 and S4 samples present the evident weight loss under air atmosphere in the temperature range of 240–620°C. Based on the XRD results, the mass loss can mainly be ascribed to the thermal decomposition of GO and CNTs, and the residual substances should be assigned to $Co_xFe_{3-x}O_4$ NPs. The TGA results indicate that the $Co_xFe_{3-x}O_4$ content in the obtained S2 and S4 samples is 18.4% and 30.4%, respectively. To confirm the composition of the obtained samples, **Figure 3B** provides their XPS spectra. It can be deduced that all the obtained NCs have four peaks located at 284, 530, 712, and 781 eV, respectively. Further, these peaks can be assigned to C 1s, O 1s, Fe 2p, and Co 2p.

To obtain the chemical valence states of Fe and Co, **Figure 4A** provides the high-resolution XPS spectra of Fe 2p. Four peaks, which are at ca. 711.2, 719.3, 724.6, and 731.4 eV, respectively,

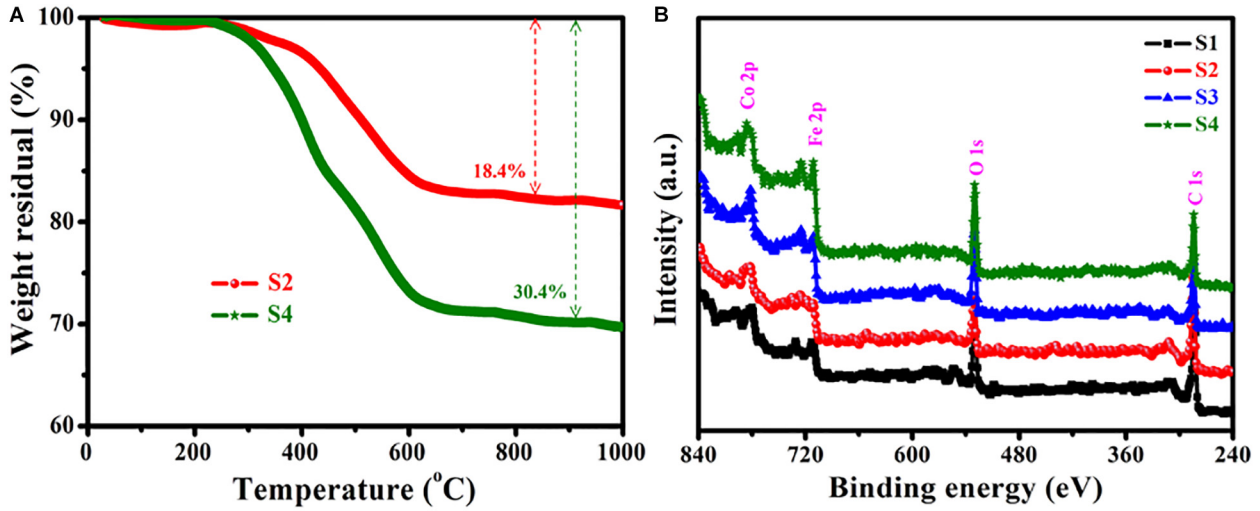

FIGURE 3 | (A) TGA curves, and **(B)** XPS spectra of the obtained samples.

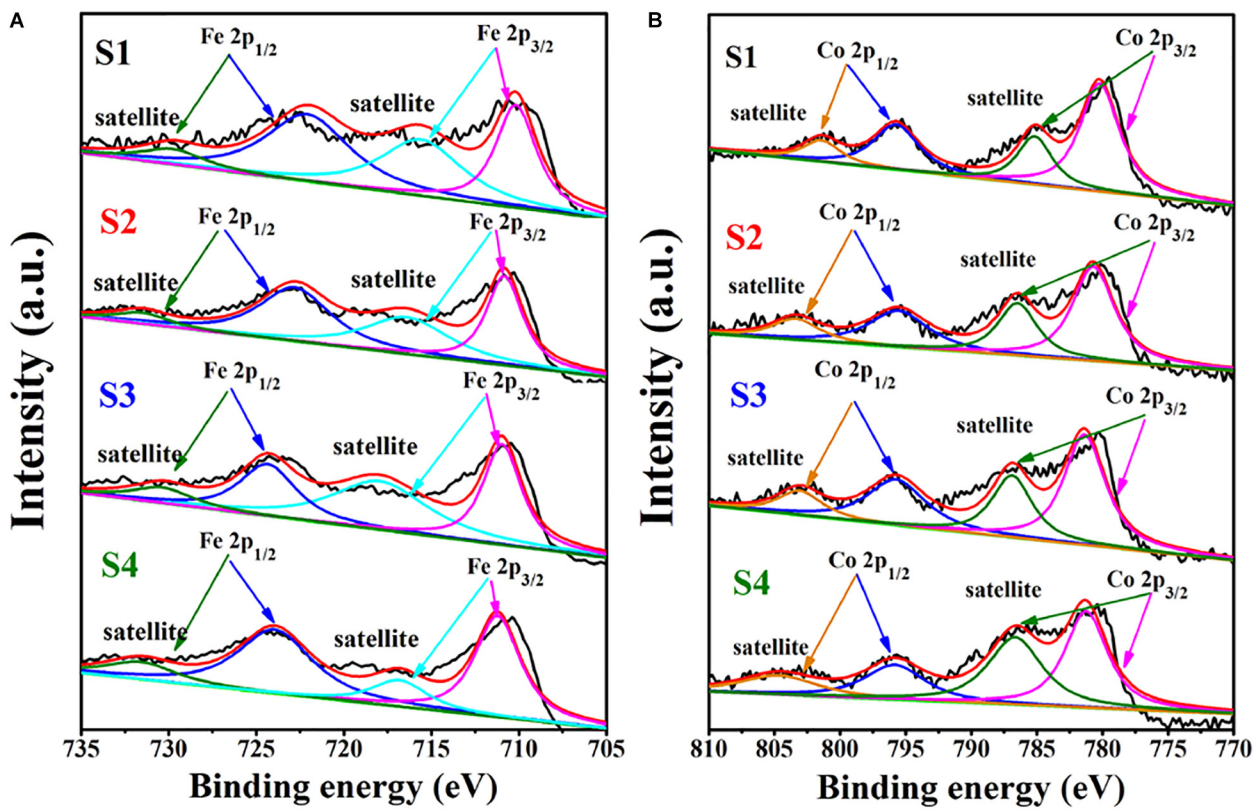

FIGURE 4 | High resolution XPS spectra of **(A)** Fe 2p, and **(B)** Co 2p peaks for the as-prepared samples.

can be observed. Among these peaks, 711.2 and 724.6 eV can be assigned to the Fe $2p_{3/2}$ and Fe $2p_{1/2}$, while the other peaks correspond to the satellite peaks of Fe $2p_{3/2}$ and Fe $2p_{1/2}$. Similarly to the previous result (Yamashita and Hayes, 2008), the obtained result suggests the presence of Fe^{3+} in the obtained samples. As indicated in **Figure 4B**, the Co 2p high-resolution spectra also display four evident peaks. The peaks located at 780.9 and 796.6 eV originate from Co $2p_{3/2}$ and Co $2p_{1/2}$, and the peaks at 786.8 and 803.3 eV are the satellite peaks of Co $2p_{3/2}$ and Co $2p_{1/2}$, which indicate the existence of Co^{2+} ions

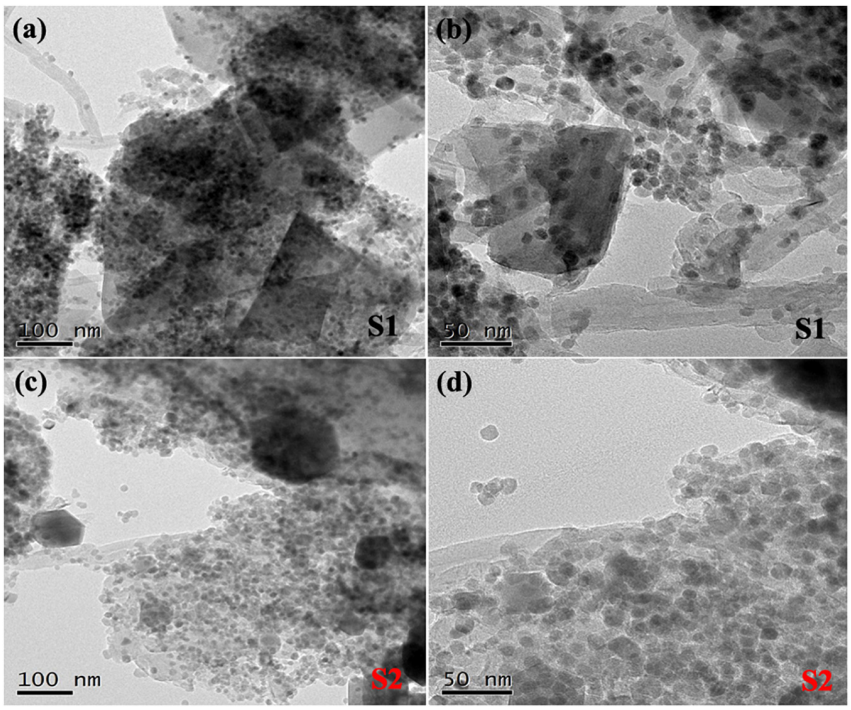

FIGURE 5 | TEM images of **(a,b)** S1, and **(c,d)** S2, respectively.

(Bennet et al., 2016). In general, the obtained XPS results are consistent with their XRD patterns.

Figure 5 provides the morphologies of the as-prepared S1 and S2. As shown in **Figure 5a,b** it can be observed that larger quantities of $Co_xFe_{3-x}O_4$ and $CoCO_3$ NPs attached on the surface of GO and CNTs, similarly to the reported GO/CNT-Fe_3O_4 NCs (Wang et al., 2014). A closer TEM observation indicates that the NPs, CNTs, and GO nanosheets are well connected with each other to form a good three dimensional (3D) hierarchical networks structure. In the same manner as S1, as displayed in **Figures 5c,d**, the obtained S2 consists of large numbers of NPs, CNTs and paper-like GO, which presents a typical structure of 3D hierarchical networks. Combined with the XRD and XPS results, the conclusion suggests that the as-prepared S1 and S2 are 3D hierarchical networks structure of $CoCO_3$-$Co_xFe_{3-x}O_4$/CNTs/GO quaternary NCs. Equally, the TEM investigation of S3 and S4 (as presented in **Figure 6**) shows that they are composed of $Co_xFe_{3-x}O_4$ NPs with a relatively uniform size, CNTs and GO nanosheets, which bind together to establish the structure of 3D hierarchical networks. Unlike S1 and S2, the XRD, XPS and TEM results demonstrate that the as-prepared S3 and S4 are 3D hierarchical networks structure of $Co_xFe_{3-x}O_4$/CNTs/GO ternary NCs. Generally, with the Co:Fe increasing from 1:1 to 1:5, it is discovered that the prepared samples gradually undergo the transition from $CoCO_3$-$Co_xFe_{3-x}O_4$/CNTs/GO quaternary NCs to $Co_xFe_{3-x}O_4$/CNTs/GO ternary NCs, which is in agreement with our reported results (Wu et al., 2020). Compared to the binary NCs such as $Co_xFe_{3-x}O_4$/CNTs and $Co_xFe_{3-x}O_4$/GO, it is well recognized that the formed $CoCO_3$-$Co_xFe_{3-x}O_4$/CNTs/GO quaternary NCs and $Co_xFe_{3-x}O_4$/CNTs/GO ternary NCs can provide many more interface contacts. Further, the generated 3D hierarchical networks structure of our designed magnetic CNTs/GO NCs can provide a double loss mechanism and synergy effect among them, which is conducive to the attenuation of the EM wave. Generally, based on the previously reported papers and our obtained results (Lu et al., 2018; Shi et al., 2018), one can find that $CoCO_3$ will easily form under the condition of the existence of urea and a small quantity of Fe source. With the increasing amounts of Fe source, much more Co^{2+} will couple with Fe^{3+} to generate the $Co_xFe_{3-x}O_4$. Therefore, the obtained S2 should display a much higher content of CNTs/GO compared to S1. Moreover, with the formation of $Co_xFe_{3-x}O_4$ with large quantities, the obtained S3 has a larger $Co_xFe_{3-x}O_4$ content compared to S2.

It is well known that the value of minimum reflection loss (RL_{min}) and its corresponding frequency bandwidth (FB_{cor}), with the reflection loss (RL) values lower than −10 dB (90% EM wave absorption) are the important characteristic for measuring high performance MAs (Ye et al., 2018). Further, it is very desirable that MAs can simultaneously have a low RL_{min} and large FB_{cor} values. To investigate their MAPs, the values of RL were calculated based on the measured EM parameters and transmission line theory (Yusoff et al., 2002):

$$Z_{in} = Z_0\sqrt{\frac{\mu}{\varepsilon}}\tanh\left(j\frac{2\pi fd\sqrt{\mu\varepsilon}}{c}\right) \quad (1)$$

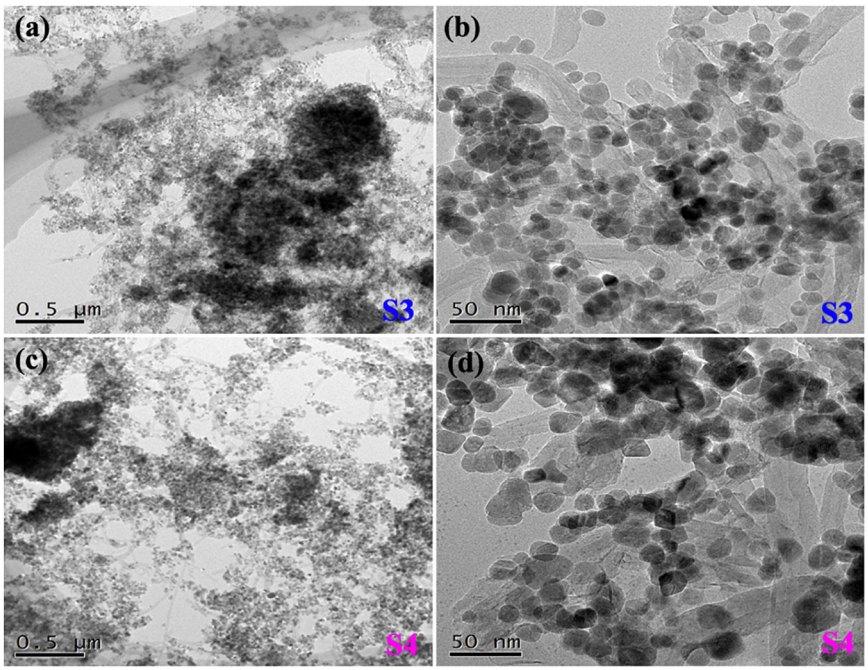

FIGURE 6 | TEM images of **(a,b)** S3, and **(c,d)** S4, respectively.

$$RL = 20\log\left|\frac{Z_{in} - Z_0}{Z_{in} + Z_0}\right| \quad (2)$$

Where f is the frequency of the EM wave, d is the thickness of absorber, c is the velocity of light, Z_0 is the impedance of air, and Z_{in} is the input impedance of absorber. **Figure 7** provides the RL curves of S1, S2, and S3. As shown in **Figures 7A,B**, the RL_{min} and large FB_{cor} values for S1 are −54.69 dB at 11.08 GHz with the matching thickness (d_m) value of 8.57 mm and 2.36 GHz. The as-prepared S2 presents the RL_{min} value of −63.99 dB at 14.96 GHz with the d_m value of 6.60 mm (**Figure 7C**), and the FB_{cor} value of 2.48 GHz (**Figure 7D**), respectively. Equally, as shown in **Figures 7E,F**, one can find that the RL_{min} value for S3 is ca. −63.36 dB at 13.12 GHz with the d_m value of 7.95 mm, and its FB_{cor} value is 2.68 GHz. Moreover, the corresponding maximum absorption bandwidths (AB_{max}) with RL < −10 dB for S1, S2, and S3 (as provided in **Figure 8**) are 2.60 GHz with the d_m value of 7.69 mm, 2.72 GHz with the d_m value of 6.00 mm, and 3.08 GHz with the d_m value of 6.33 mm, respectively. In general, the designed magnetic CNTs/GO NCs display very outstanding MAPs. The as-prepared S3 exhibits the superior comprehensive MAPs compared to S1 and S2. As summarized in **Figure 9**, the proposed magnetic CNTs/GO NCs present excellent comprehensive MAPs compared to the representative related NCs reported previously (Li et al., 2015; Yang et al., 2016; Zhang et al., 2016; Zhang K.C. et al., 2017; Zhang S. et al., 2017; Ren et al., 2018; Shu et al., 2018a,b; Hu et al., 2019; Lu et al., 2019; Xu et al., 2019).

To effectively understand their MAPs, **Figure 10** gives their complex permittivity $(\varepsilon = \varepsilon' - j\varepsilon'')$ and complex permeability $(\mu = \mu' - j\mu'')$. As shown in **Figures 10A,B**, besides the shift of peak at ca. 13 GHz, the as-prepared samples present the similar ε' and ε'' variation tendency in the frequency region owing to the same categories of samples. The complex permittivity exhibits several resonant peaks in the whole frequency range, indicating the multiple relaxation processes (Huang et al., 2019). Furthermore, the ε' and ε'' values of samples present the decreased tendency with the frequency increasing from 2 to 18 GHz, which can be explained by the Debye theory (Wang et al., 2015). Overall, the obtained S2 has larger values of ε' and ε'' compared to S1 and S3, which can be ascribed to the highest content of CNTs/GO in the as-prepared S2. According to the previous result (Li et al., 2017), the ε' and ε'' values could be effectively enhanced by increasing the content of CNTs. The obtained S3 presents the lowest values of ε' and ε'', which should be ascribed to the gradual formation of $Co_xFe_{3-x}O_4$ with large quantities in NCs resulting in the decreasing content of CNTs/GO. **Figures 10C,D** present the μ' and μ'' values of the obtained samples. Generally, it can be observed that the obtained samples exhibit the gradually growing μ' and μ'' values with increased addition of Fe sources, which can be related to the enhanced content of $Co_xFe_{3-x}O_4$ NPs in the NCs. **Figure 11** provides the dielectric loss ($\tan\delta_E = \varepsilon''/\varepsilon'$) and magnetic capabilities ($\tan\delta_m = \mu''/\mu'$). Overall, the as-prepared magnetic CNTs/GO NCs display much higher $\tan\delta_E$ values than those of $\tan\delta_m$, which indicates that the attenuation of wave EM mainly originates from dielectric loss (Feng et al., 2020; Li et al., 2020). Moreover, the obtained S2 displays larger values of $\tan\delta_E$ compared to S1 and S3. Further, the large

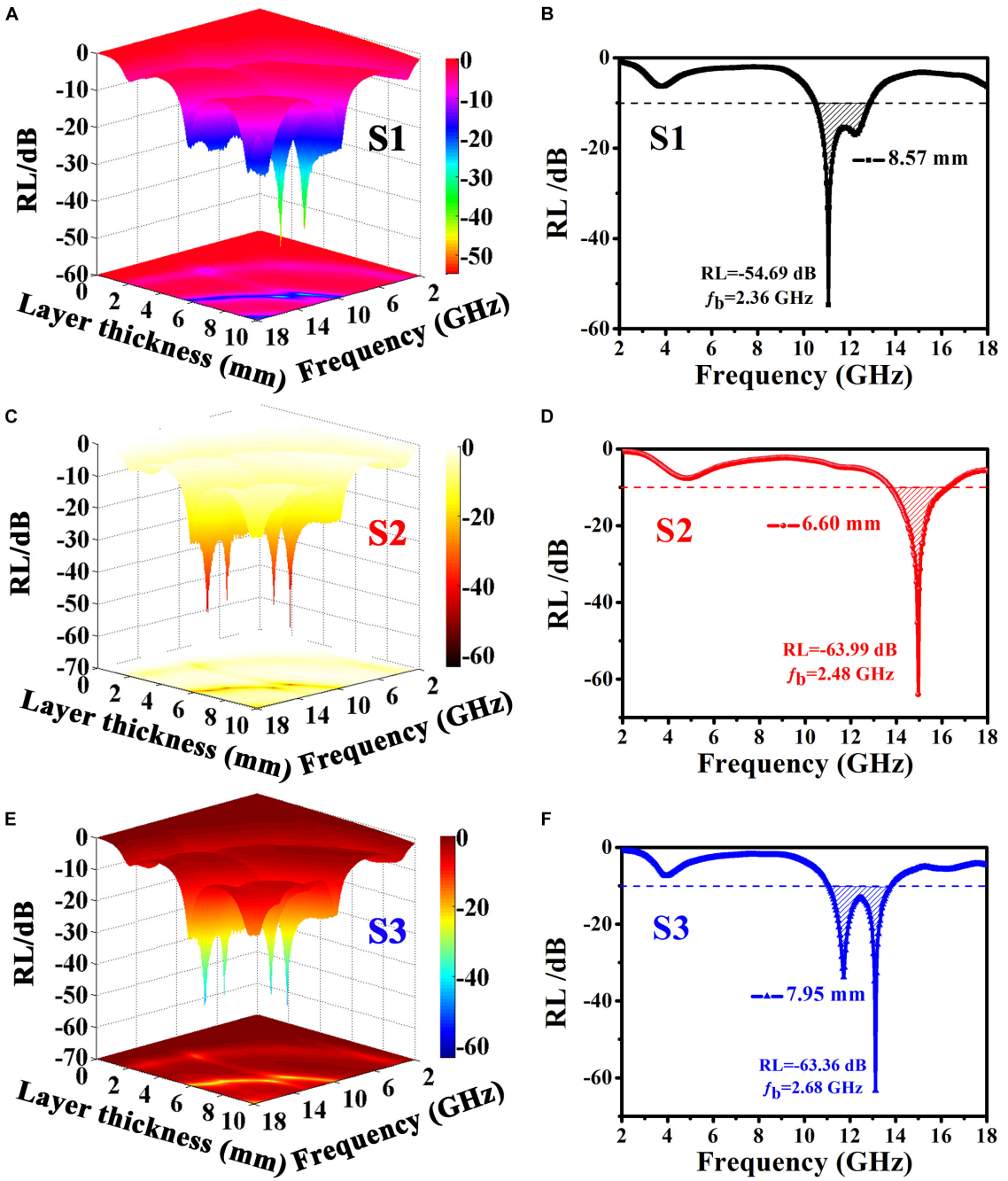

FIGURE 7 | 3D color RL curves and their corresponding RL_{min} plots of **(A,B)** S1, **(C,D)** S2, and **(E,F)** S3.

$\tan\delta_m$ values of S3 are higher than those of S1 and S2. The difference in dielectric loss and magnetic loss abilities should be related to the different CNTs/GO and magnetic $Co_xFe_{3-x}O_4$ NPs contents.

Based on the obtained EM parameters, RL curves and the previously reported mechanisms for the interpretation of the good MAPs (Liu et al., 2012, 2020), the excellent MAPs of the as-prepared magnetic CNTs/GO NCs can be explained by the geometrical effect. For this model, the values of d_m and peak frequency (f_m) should satisfy the 1/4 wavelength equation (Liu et al., 2020):

$$d_m = nc \Big/ 4f_m\sqrt{|\mu||\varepsilon|} \quad (n = 1, 3, 5\cdots) \tag{3}$$

Figure 12 provides their comparison results between the experimental value of d_m^{exp} (obtaining directly from their RL curves) and their theoretical curves of d_m^{sim} [plotting by the formula (3)]. One can find that the scattered dots of d_m^{exp} land on

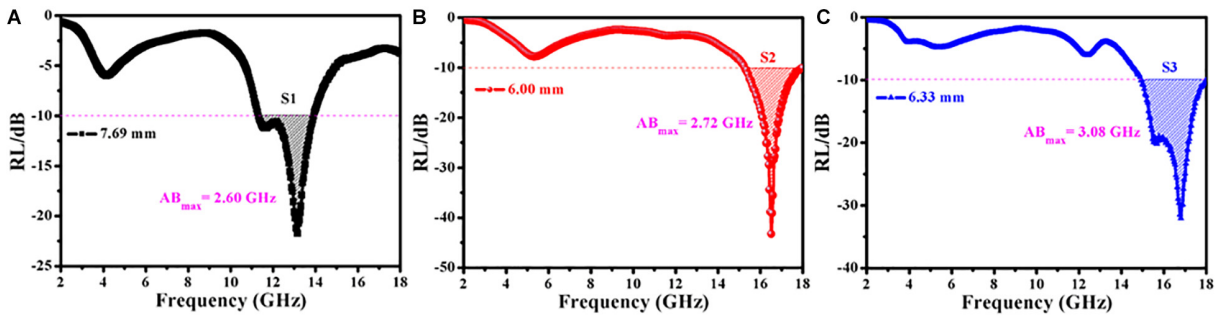

FIGURE 8 | Typical RL curves versus frequency plots for **(A)** S1, **(B)** S2, and **(C)** S3, respectively.

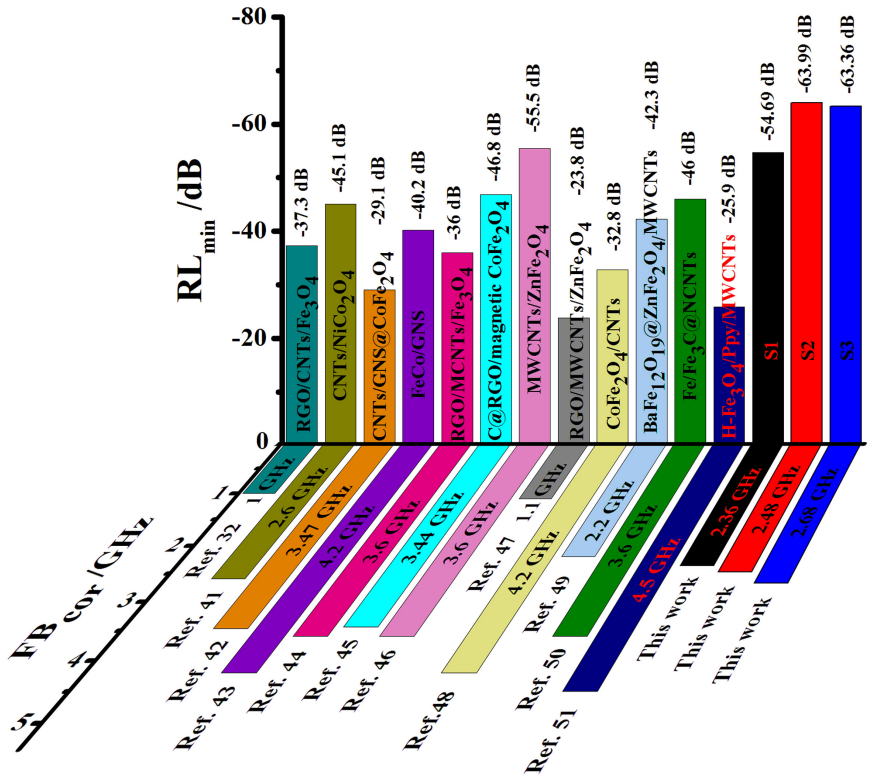

FIGURE 9 | Comparison results of MAPs with the representative NCs reported in recent papers.

the theoretical curves of d_m^{sim}. Consistent with the CoNi@PRM-NC, $ZnFe_2O_4$@C, and CNTs@MoS_2 reported elsewhere (Gao et al., 2019; Yan et al., 2019; Wang et al., 2020), the agreement between the experimental and theoretical values suggests the cancelation effect of reflected EM waves and a strong EM wave attenuation.

Based on the previous models and our obtained results (Wang et al., 2014; Shu et al., 2018a), as depicted in **Figure 13**, as for our designed magnetic CNTs/GO NCs, the possible paths for the EM wave attenuation are mainly attributed to the following facts: (i) the 3D hierarchical networks structure results in the multiple reflections and/or scattering of the EM wave (**Figure 13A**), which plays a significant role in the EM wave attenuation; (ii) many more interface contacts among magnetic NPs, CNTs, and GO nanosheets (**Figure 13B**) induce the formation of interface polarization with large quantities, which can effectively dissipate the energy of the incident EM wave; (iii) the designed NCs consisted of dielectric substances and magnetic NPs (**Figure 13C**), which can simultaneously provide the dielectric and magnetic loss mechanism. The excellent synergistic effect between them further improves the attenuation of the EM wave; (iv) the high conductivity of GO/CNT and a large number of defects and functional groups existing on CNTs (**Figure 13B**) and GO (**Figure 13D**) can generate massive electrons, defect dipoles and interface polarizations, which are also conducive of the dissipation of the EM wave.

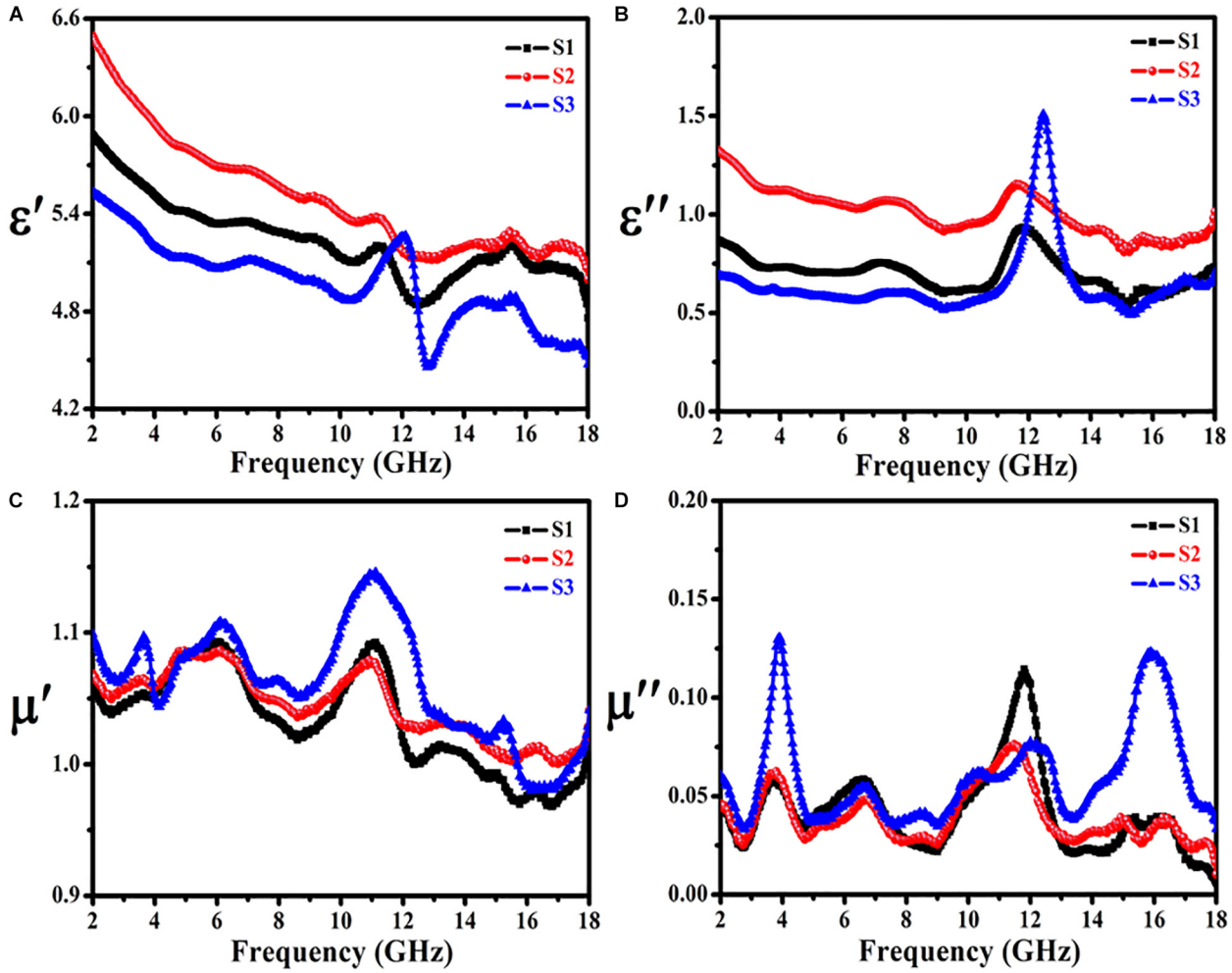

FIGURE 10 | EM parameters for the as-prepared samples: **(A,B)** complex permittivity, and **(C,D)** complex permeability.

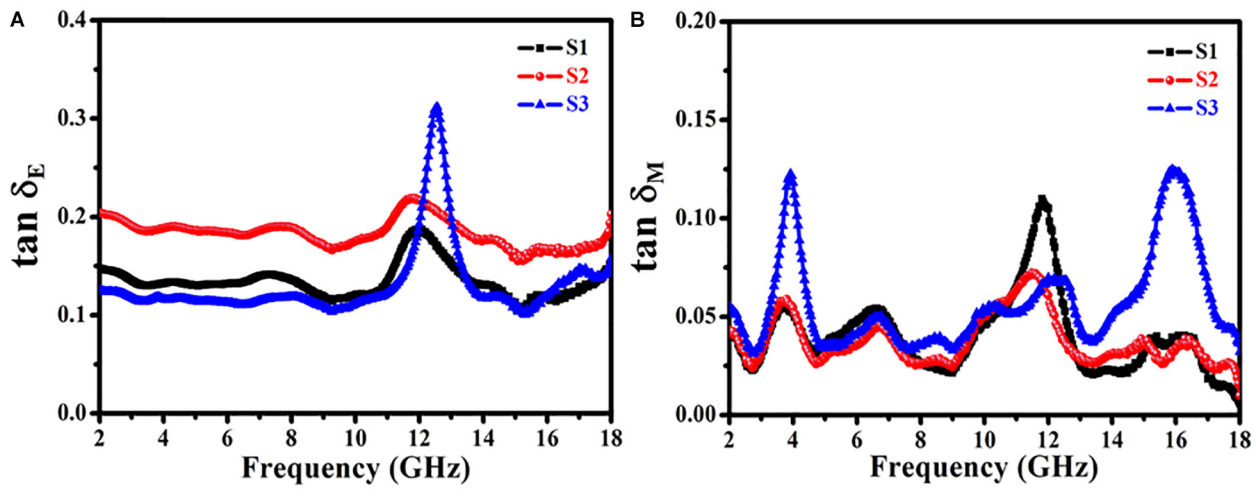

FIGURE 11 | Frequency dependence **(A)** dielectric loss tangent, and **(B)** magnetic loss tangent of the as-prepared samples.

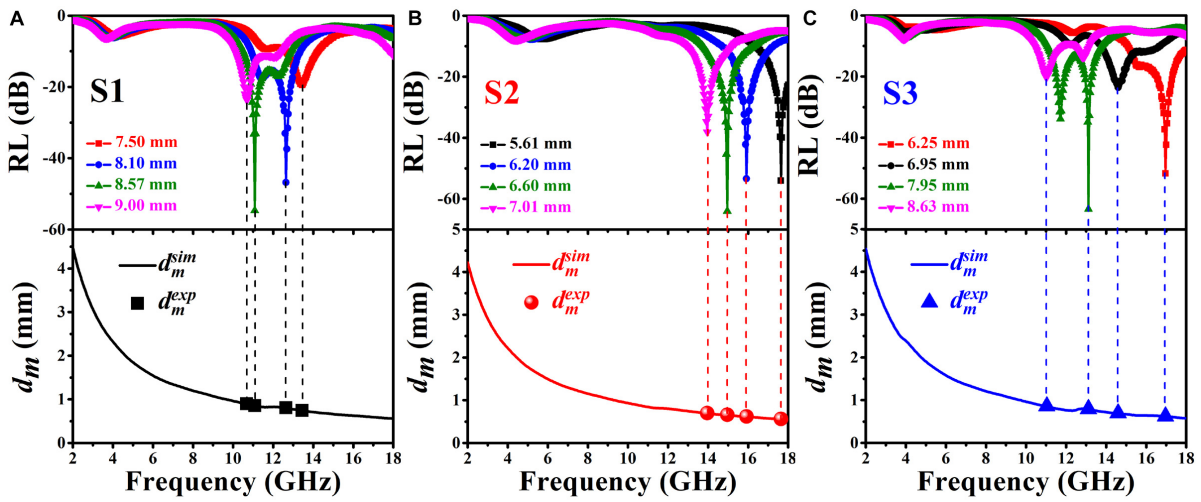

FIGURE 12 | Comparison results between the calculated and experimental matching thicknesses for **(A)** S1, **(B)** S2, and **(C)** S3.

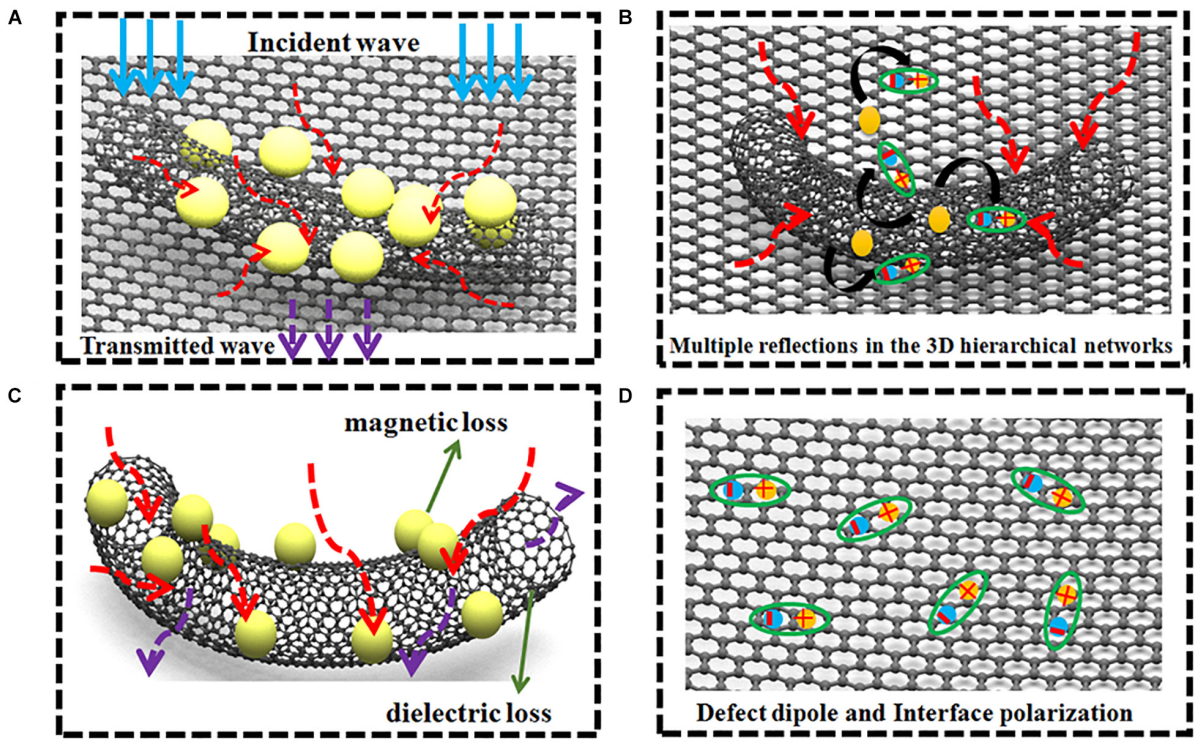

FIGURE 13 | Schematic illustration of possible EM wave absorption avenues of magnetic CNTs/GO NCs. **(A,B)** Multiple reflections, **(C)** dielectric and magnetic loss, and **(D)** defect dipole and interface polarization.

CONCLUSION

In summary, we proposed a one-step hydrothermal method to selectively synthesize different compositions of magnetic CNTs/GO NCs such as $CoCO_3$-$Co_xFe_{3-x}O_4$/CNTs/GO quaternary NCs and $Co_xFe_{3-x}O_4$/CNTs/GO ternary NCs. The TEM investigation indicated that the designed NC consisted of $CoCO_3$-$Co_xFe_{3-x}O_4$ NPs, CNTs, and GO nanosheets, which were well bound together to form the good 3D hierarchical networks structure. Owing to the construction of many more interface contacts among magnetic NPs, CNTs, and GO nanosheets, an excellent synergistic effect between dielectric and magnetic loss substances, the as-prepared magnetic CNTs/GO NCs presented very extraordinary MAPs. The RL_{min} and

FB_{cor} values for the as-prepared samples were ca. −54.69 dB and 2.36 GHz, −63.99 dB and 2.48 GHz, −63.36 dB and 2.68 GHz, respectively. Moreover, owing to their low cost, lightweight and high stability, the proposed 3D hierarchical networks structures of magnetic GO/CNTs NCs exhibit very outstanding comprehensive MAPs, which may be used as promising candidates for high performance MAs and are very much worth further study.

DATA AVAILABILITY STATEMENT

The raw data supporting the conclusions of this article will be made available by the authors, without undue reservation, to any qualified researcher.

AUTHOR CONTRIBUTIONS

MW contributed to the conceptualization, methodology, investigation and provided resources. XQ contributed to the conceptualization, methodology and writing of the original draft of the manuscript. RX contributed to the investigation. SQ provided supervision, and contributed to the writing, review and editing of the manuscript. CD provided formal analysis and resources. WZ contributed to the methodology, and the writing, review and editing of the manuscript.

FUNDING

This work was supported by the Fund of Fok Ying Tung Education Foundation, the Platform of Science and Technology and Talent Team Plan of Guizhou Province (2017-5610 and 2017-5788), the Major Research Project of Innovative Group of Guizhou Province (2018-013), the National Science Foundation of Guizhou Province (2017-1034), and the National Natural Science Foundation of China (Grant Nos. 11474151, 11604060, and 11964006) for financial support.

REFERENCES

Bennet, J., Tholkappiyan, R., Vishista, K., Jaya, N. V., and Hamed, F. (2016). Attestation in self-propagating combustion approach of spinel AFe(2)O(4) (A = Co, Mg and Mn) complexes bearing mixed oxidation states: magnetostructural properties. *App. Sur. Sci.* 383, 113–125. doi: 10.1016/j.apsusc.2016.04.177

Cao, M. S., Wang, X. X., Zhang, M., Shu, J. C., Cao, W. Q., Yang, H. J., et al. (2019). Electromagnetic response and energy conversion for functions and devices in low-dimensional materials. *Adv. Funct. Mater.* 25:1807398. doi: 10.1002/adfm.201807398

Che, R. C., Peng, L. M., Duan, X. F., and Chen, Q. (2004). Microwave absorption enhancement and complex permittivity and permeability of Fe encapsulated within carbon nanotubes. *Adv. Mater.* 16, 401–405. doi: 10.1002/adma.200306460

Chen, N., Jiang, J. T., Xu, C. Y., Yuan, Y., Gong, Y. X., and Zhen, L. (2017). Co7Fe3 and Co7Fe3@SiO2 nanospheres with tunable diameters for high-performance electromagnetic wave absorption. *ACS Appl. Mater. Interfaces* 9, 21933–21941. doi: 10.1021/acsami.7b03907

Chen, Y. H., Huang, Z. H., Lu, M. M., Cao, W. Q., Yuan, J., Zhang, D. Q., et al. (2015). 3D Fe3O4 nanocrystals decorating carbon nanotubes to tune electromagnetic properties and enhance microwave absorption capacity. *J. Mater. Chem. A* 3, 12621–12625. doi: 10.1039/C5TA02782A

Fang, J. Y., Liu, T., Chen, Z., Wang, Y., Wei, W., Yue, X. G., et al. (2016). A wormhole-like porous carbon/magnetic particles composite as an efficient broadband electromagnetic wave absorber. *Nanoscale* 8, 8899–8909. doi: 10.1039/C6NR01863G

Feng, A. L., Hou, T. Q., Jia, Z. R., and Wu, G. L. (2020). Synthesis of a hierarchical carbon fiber@cobalt ferrite@manganese dioxide composite and its application as a microwave absorber. *RSC Adv.* 10, 10510–10518. doi: 10.1039/C9RA10327A

Gao, Z. G., Xu, B. H., Ma, M. L., Feng, A. L., Zhang, Y., Liu, X. H., et al. (2019). Electrostatic self-assembly synthesis of ZnFe2O4 quantum dots (ZnFe2O4@C) and electromagnetic microwave absorption. *Composites B Eng.* 179:107417. doi: 10.1016/j.compositesb.2019.107417

Hu, Q. M., Yang, R. L., Mo, Z. C., Lu, D. W., Yang, L. L., He, Z. F., et al. (2019). Nitrogen-doped and Fe-filled CNTs/NiCo2O4 porous sponge with tunable microwave absorption performance. *Carbon* 153, 737–744. doi: 10.1016/j.carbon.2019.07.077

Huang, L., Li, J. J., Wang, Z. J., Li, Y. B., He, X. D., and Yuan, Y. (2019). Microwave absorption enhancement of porous C@CoFe2O4 nanocomposites derived from eggshell membrane. *Carbon* 143, 507–516. doi: 10.1016/j.carbon.2018.11.042

Hummers, W. S., and Offeman, R. E. (1958). Preparation of graphitic oxide. *J. Am. Chem. Soc.* 80:1339. doi: 10.1021/ja01539a017

Jiang, J. J., Li, D., Geng, D. Y., An, J., He, J., Liu, W., et al. (2014). Microwave absorption properties of core double-shell FeCo/C/BaTiO3 nanocomposites. *Nanoscale* 6, 3967–3971. doi: 10.1039/C3NR04087A

Khabouri, S. A., Harthi, S. A., Maekawa, T., Nagaoka, Y., Hinai, A. A., et al. (2015). Composition, electronic and magnetic investigation of the encapsulated ZnFe2O4 nanoparticles in multiwall carbon nanotubes containing Ni residuals. *Nanoscale Res. Lett.* 10:262. doi: 10.1186/s11671-015-0971-7

Li, N., Huang, G. W., Li, Y. Q., Xiao, H. M., Feng, Q. P., Hu, N., et al. (2017). Enhanced microwave absorption performance of coated carbon nanotubes by optimizing the Fe3O4 nanocoating structure. *ACS Appl. Mater. Interfaces* 9, 2973–2983. doi: 10.1021/acsami.6b13142

Li, X., Yu, L. M., Zhao, W. K., Shi, Y. Y., Yu, L. J., Dong, Y. B., et al. (2020). Prism-shaped hollow carbon decorated with polyaniline for microwave absorption. *Chem. Eng. J.* 379:122393. doi: 10.1016/j.cej.2019.122393

Li, X. H., Feng, J., Du, Y. P., Bai, J. T., Fan, H. M., Zhang, H. L., et al. (2015). One-pot synthesis of CoFe2O4/graphene oxide hybrids and their conversion into FeCo/graphene hybrids for lightweight and highly efficient microwave absorber. *J. Mater. Chem. A* 3, 5535–5546. doi: 10.1039/C4TA05718J

Liu, J. W., Che, R. C., Chen, H. J., Zhang, F., Xia, F., Wu, Q. S., et al. (2012). Microwave absorption enhancement of multifunctional composite microspheres with spinel Fe3O4 cores and anatase TiO2 shells. *Small* 8, 1214–1221. doi: 10.1002/smll.201102245

Liu, P. B., Gao, S., Huang, W. H., Ren, J., Yu, D. Y., and He, W. J. (2020). Hybrid zeolite imidazolate framework derived N-implanted carbon polyhedrons with tunable heterogeneous interfaces for strong wideband microwave attenuation. *Carbon* 159, 83–93. doi: 10.1016/j.carbon.2019.12.021

Liu, Q. H., Cao, Q., Bi, H., Liang, C. Y., Yuan, K. P., She, W., et al. (2016). CoNi@SiO2@TiO2 and CoNi@Air@TiO2 microspheres with strong wideband microwave absorption. *Adv. Mater.* 28, 486–490. doi: 10.1002/adma.201503149

Liu, X., Chen, Y., Cui, X., Zeng, M., Yu, R., and Wang, G. S. (2015). Flexible nanocomposites with enhanced microwave absorption properties based on Fe3O4/SiO2 nanorods and polyvinylidene fluoride. *J. Mater. Chem. A* 3, 12197–12204. doi: 10.1039/C5TA01924A

Liu, X. F., Hao, C. C., He, L. H., Yang, C., Chen, Y. B., Jiang, C. B., et al. (2018). Yolk-shell structured Co-C/void/Co9S8 composites with a tunable cavity for ultrabroadband and efficient low-frequency microwave absorption. *Nano Res.* 11, 4169–4182. doi: 10.1007/s12274-018-2006-z

Liu, X. G., Geng, D. Y., Meng, H., Shang, P. J., and Zhang, Z. D. (2008). Microwave-absorption properties of ZnO coated iron nanocapsules. *Appl. Phys. Lett.* 92, 64–67. doi: 10.1063/1.2919098

Long, L., Yang, E. Q., Qi, X. S., Xie, R., Bai, Z. C., Qin, S. J., et al. (2019). Core@shell structured flower-like Co0.6*Fe*2.4O4@MoS2 nanocomposites: a strong absorption and broadband electromagnetic wave absorber. *J. Mater. Chem. C* 7, 8975–8981. doi: 10.1039/C9TC02140J

Long, L., Yang, E. Q., Qi, X. S., Xie, R., Qin, S. J., Deng, C. Y., et al. (2020). Positive and reverse core/shell structure CoxFe3-xO4/MoS2 and MoS2/CoxFe3-xO4 nanocomposites: selective production and outstanding electromagnetic absorption comprehensive performance. *ACS Sustain. Chem. Eng.* 8, 613–623. doi: 10.1021/acssuschemeng.9b06205

Lu, M. J., Wang, J., Su, X. G., Wu, Q. L., Yan, T. Y., and Zhang, X. X. (2019). Fabrication, structure, and microwave absorbing properties of plate-like BaFe12O19@ZnFe2O4/MWCNTs nanocomposites. *Mater. Lett.* 253, 46–49. doi: 10.1016/j.matlet.2019.06.012

Lu, Z. P., Wang, H., Zhou, T., Ma, C., Yin, F., Jiang, X. F., et al. (2018). CoCO3 micrometer particles stabilized by carbon nanofibers networks as composite electrode for enhanced rate and cyclic performance of lithium-ion batteries. *Electrochim. Acta* 270, 22–29. doi: 10.1016/j.electacta.2018.03.081

Lv, R. T., Kang, F. Y., Gu, J. L., Gui, X. C., Wei, J. Q., Wang, K. L., et al. (2008). Carbon nanotubes filled with ferromagnetic alloy nanowires: lightweight and wide-band microwave absorber. *Appl. Phys. Lett.* 93:223105. doi: 10.1063/1.3042099

Novoselov, K. S., Geim, A. K., Morozov, S. V., Dubonos, S. V., Zhang, Y., and Jiang, D. (2004). Electric field effect in atomically thin carbon films. *Science* 306, 666–669. doi: 10.1126/science.1102896

Pawar, S. P., Melo, G., and Sundararaj, U. (2019). Dual functionality of hierarchical hybrid networks of multiwall carbon nanotubes anchored magnetite particles in soft polymer nanocomposites: simultaneous enhancement in charge storage and microwave absorption. *Compos. Sci. Technol.* 183:107802. doi: 10.1016/j.compscitech.2019.107802

Popov, V. N., and Lambin, P. (2013). Theoretical Raman intensity of the G and 2D bands of strained graphene. *Carbon* 54, 86–93. doi: 10.1016/j.carbon.2012.11.006

Qu, B., Zhu, C. L., Li, C. Y., Zhang, X. T., and Chen, Y. J. (2016). Coupling hollow Fe3O4-Fe nanoparticles with graphene sheets for high-performance electromagnetic wave absorbing material. *ACS Appl. Mater. Interfaces* 8, 3730–3735. doi: 10.1021/acsami.5b12789

Quan, B., Liang, X. H., Ji, G. B., Ma, J. N., Ouyang, P. Y., Gong, H., et al. (2017). Strong electromagnetic wave response derived from the construction of dielectric/magnetic media heterostructure and multiple interfaces. *ACS Appl. Mater. Interfaces* 9, 9964–9974. doi: 10.1021/acsami.6b15788

Ren, F., Guo, Z. Z., Shi, Y. F., Jia, L. C., Qing, Y. C., Ren, P. G., et al. (2018). Lightweight and highly efficient electromagnetic wave-absorbing of 3D CNTs/GNS@CoFe2O4 ternary composite aerogels. *J. Alloy Compd.* 786, 6–14. doi: 10.1016/j.jallcom.2018.07.209

Ritter, U., Scharff, P., Siegmund, C., Dmytrenko, O. P., Kulish, N. P., Prylutskyy, Y. I., et al. (2006). Radiation damage to multi-walled carbon nanotubes and their Raman vibrational modes. *Carbon* 44, 2694–2700. doi: 10.1016/j.carbon.2006.04.010

Shi, S. J., Zhang, M., Liu, Y. Y., Hua, X. Y., Guo, H. T., and Yang, G. (2018). Efficient construction of a CoCO3/graphene composite anode material for lithium-ion batteries by stirring solvothermal reaction. *Ceram. Int.* 44, 3718–3725. doi: 10.1016/j.ceramint.2017.11.152

Shu, R. W., Li, W. J., Zhou, X., Tian, D. D., Zhang, G. Y., Gan, Y., et al. (2018a). Facile preparation and microwave absorption properties of RGO/MWCNTs/ZnFe2O4 hybrid nanocomposites. *J. Alloy Compd.* 743, 163–174. doi: 10.1016/j.jallcom.2018.02.016

Shu, R. W., Zhang, G. Y., Wang, X., Gao, X., Wang, M., Gan, Y., et al. (2018b). Fabrication of 3D net-like MWCNTs/ZnFe2O4 hybrid composites as high-performance electromagnetic wave absorbers. *Chem. Eng. J.* 337, 242–255. doi: 10.1016/j.cej.2017.12.106

Wang, C., Murugadoss, V., Kong, J., He, Z. F., Mai, X. M., Shao, Q., et al. (2018). Overview of carbon nanostructures and nanocomposites for electromagnetic wave shielding. *Carbon* 140, 696–733. doi: 10.1016/j.carbon.2018.09.006

Wang, G. Z., Gao, Z., Tang, S. W., Chen, C. Q., Duan, F. F., Zhao, S. C., et al. (2012). Microwave absorption properties of carbon nanocoils coated with highly controlled magnetic materials by atomic layer deposition. *ACS Nano* 6, 11009–11017. doi: 10.1021/nn304630h

Wang, L. N., Jia, X. L., Li, Y. F., Yang, F., Zhang, L. Q., Liu, L. P., et al. (2014). Synthesis and microwave absorption property of flexible magnetic film based on graphene oxide/carbon nanotubes and Fe3O4 nanoparticles. *J. Mater. Chem. A* 2, 14940–14946. doi: 10.1039/C4TA02815E

Wang, R., Yang, E. Q., Qi, X. S., Xie, R., Qin, S. J., Deng, C. Y., et al. (2020). Constructing and optimizing core@shell structure CNTs@MoS2 nanocomposites as outstanding microwave absorbers. *Appl. Surf. Sci.* 516:146159. doi: 10.1016/j.apsusc.2020.146159

Wang, Y., Gao, X., Wu, X. M., Zhang, W. Z., Luo, C. Y., and Liu, P. B. (2019). Facile design of 3D hierarchical NiFe2O4/N-GN/ZnO composite as a high performance electromagnetic wave absorber. *Chem. Eng. J.* 375:121942. doi: 10.1016/j.cej.2019.121942

Wang, Y. F., Chen, D. L., Yin, X., Xu, P. F., and He, M. (2015). Hybrid of MoS2 and reduced graphene oxide: a lightweight and broadband electromagnetic wave absorber. *ACS Appl. Mater. Interfaces* 7, 26226–26234. doi: 10.1021/acsami.5b08410

Wei, S., Wang, X. X., Zhang, B. Q., Yu, M. G., Zheng, Y. W., Wang, Y., et al. (2017). Preparation of hierarchical core-shell C@NiCo2O4@Fe3O4 composites for enhanced microwave absorption performance. *Chem. Eng. J.* 314, 477–487. doi: 10.1016/j.cej.2016.12.005

Weissker, U., Hampel, S., Leonhardt, A., and Büchner, B. (2010). Carbon nanotubes filled with ferromagnetic materials. *Materials* 3, 4387–4427. doi: 10.3390/ma3084387

Wen, F. S., Zhang, F., and Liu, Z. Y. (2011). Investigation on microwave absorption properties for multiwalled carbon nanotubes/Fe/Co/Ni nanopowders as lightweight absorbers. *J. Phys. Chem. C* 115, 14025–14030. doi: 10.1021/jp202078p

Wu, M., Qi, X. S., Xie, R., Bai, Z. C., Qin, S. J., Zhong, W., et al. (2020). Graphene oxide/carbon nanotubes/CoxFe3-xO4 ternary nanocomposites: controllable synthesis and their excellent microwave absorption capabilities. *J Alloy Compd.* 813:151996. doi: 10.1016/j.jallcom.2019.151996

Xu, J. L., Qi, X. S., Sun, Y., Wang, Z. C., Liu, Y., Luo, C. Z., et al. (2018). Tuning the electromagnetic synergistic effects for enhanced microwave absorption via magnetic nickel core encapsulated in hydrogenated anatase TiO2 shell. *ACS Sustain. Chem. Eng.* 6, 12046–12054. doi: 10.1021/acssuschemeng.8b02350

Xu, Z., Du, Y. C., Liu, D. W., Wang, Y. H., Ma, W. J., Wang, Y., et al. (2019). Pea-like Fe/Fe3C nanoparticles embedded in nitrogen-doped carbon nanotubes with tunable dielectric/magnetic loss and efficient electromagnetic absorption. *ACS Appl. Mater. Interfaces* 11, 4268–4277. doi: 10.1021/acsami.8b19201

Yamashita, T., and Hayes, P. (2008). Analysis of XPS spectra of Fe2+ and Fe3+ ions in oxide materials. *App. Sur. Sci.* 254, 2441–2449. doi: 10.1016/j.apsusc.2007.09.063

Yan, J., Huang, Y., Chen, C., Liu, X. D., and Liu, H. (2019). The 3D CoNi alloy particles embedded N-doped porous carbon foam for high-performance microwave absorber. *Carbon* 152, 545–555. doi: 10.1016/j.carbon.2019.06.064

Yang, R. B., Reddy, P. M., Chang, C. J., Chen, P. A., Chen, J. K., and Chang, C. C. (2016). Synthesis and characterization of Fe3O4/polypyrrole/carbon nanotube composites with tunable microwave absorption properties: role of carbon nanotube and polypyrrole content. *Chem. Eng. J.* 285, 497–507. doi: 10.1016/j.cej.2015.10.031

Ye, F., Song, Q., Zhang, Z. C., Li, W., Zhang, S. Y., Yin, X. W., et al. (2018). Direct growth of edge-rich graphene with tunable dielectric properties in porous Si3N4 ceramic for broadband high-performance microwave absorption. *Adv. Funct. Mater.* 28:1707205. doi: 10.1002/adfm.201707205

Yusoff, A. N., Abdullah, M. H., Ahmad, S. H., Jusoh, S. F., Mansor, A. A., and Hamid, S. A. A. (2002). Electromagnetic and absorption properties of some microwave absorbers. *J. Appl. Phys.* 92, 876–882. doi: 10.1063/1.1489092

Zhang, H., Hong, M., Chen, P., Xie, A. J., and Shen, Y. H. (2016). 3D and ternary rGO/MCNTs/Fe3O4 composite hydrogels: synthesis, characterization and their electromagnetic wave absorption properties. *J. Alloy Compd.* 665, 381–387. doi: 10.1016/j.jallcom.2016.01.091

Zhang, K. C., Gao, X. B., Zhang, Q., Li, T. P., Chen, H., and Chen, X. F. (2017). Preparation and microwave absorption properties of asphalt carbon coated reduced graphene oxide/magnetic CoFe2O4 hollow particles modified multi-wall carbon nanotube composites. *J. Alloy Compd.* 723, 912–921. doi: 10.1016/j.jallcom.2017.06.327

Zhang, S., Qi, Z., Zhao, Y., Jiao, Q., Ni, X., Wang, Y., et al. (2017). Core/shell structured composites of hollow spherical CoFe2O4 and CNTs as absorbing materials. *J. Alloy Compd.* 694, 309–312.

Zhang, X. J., Wang, G. S., Cao, W. Q., Wei, Y. Z., Liang, J. F., Guo, L., et al. (2014). Enhanced microwave absorption property of reduced graphene oxide (RGO)-MnFe2O4 nanocomposites and polyvinylidene fluoride. *ACS Appl. Mater. Interfaces* 6, 7471–7478. doi: 10.1021/am500862g

Zhang, Y., Huang, Y., Zhang, T. F., Chang, H. C., Xiao, P. S., Chen, H. H., et al. (2015). Broadband and tunable high-performance microwave absorption of an ultralight and highly compressible graphene foam. *Adv. Mater.* 27, 2049–2053. doi: 10.1002/adma.201405788

Zhao, B., Guo, X. Q., Zhao, W. Y., Deng, J. S., Shao, G., Fan, B. B., et al. (2016). Yolk-shell Ni@SnO2 composites with a designable interspace to improve the electromagnetic wave absorption properties. *ACS Appl. Mater. Interfaces* 8, 28917–28925. doi: 10.1021/acsami.6b10886

Conflict of Interest: The authors declare that the research was conducted in the absence of any commercial or financial relationships that could be construed as a potential conflict of interest.